HHS Public Access

Author manuscript

NMR Biomed. Author manuscript; available in PMC 2019 March 01.

Published in final edited form as:

NMR Biomed. 2018 March ; 31(3): . doi:10.1002/nbm.3887.

Development of Manganese-Enhanced Magnetic Resonance Imaging of the Rostral Ventrolateral Medulla of Conscious Rats: Importance of Normalization and Comparison to Other Regions of Interest

Daniel J. Huereca[a,+], **Konstandinos A. Bakoulas**[b,+], **Farhad Ghoddoussi**[c], **Bruce A. Berkowitz**[d,e], **Avril Genene Holt**[d,f], and **Patrick J. Mueller**[b,*]

[a]Department of Pharmacology, Wayne State University School of Medicine, Detroit, MI

[b]Department of Physiology, Wayne State University School of Medicine, Detroit, MI

[c]Department of Anesthesiology, Wayne State University School of Medicine, Detroit, MI

[d]Department of Anatomy and Cell Biology, Wayne State University School of Medicine, Detroit, MI

[e]Department of Opthlamology, Wayne State University School of Medicine, Detroit, MI

[f]John Dingell Veterans Administration Medical Center, Detroit, MI

Abstract

Spinally-projecting neurons in the rostral ventrolateral medulla (RVLM) are believed to contribute to pathophysiological alterations in sympathetic nerve activity and the development of cardiovascular disease. The ability to identify changes in the activity of RVLM neurons in conscious animals and humans, especially longitudinally, would represent a clinically important advancement in understanding of the RVLM's contribution to cardiovascular disease. To this end, we describe the initial development of manganese-enhanced magnetic resonance imaging (MEMRI) for the rat RVLM. Manganese (Mn^{2+}) has been used to estimate *in vivo* neuronal activity in other brain regions due to both its paramagnetic properties and its entry into and accumulation in active neurons. In this initial study, our three goals were to: 1) validate that Mn^{2+} enhancement occurs in functionally- and anatomically-localized images of the rat RVLM; 2) quantify the dose and time course dependency of Mn^{2+} enhancement in the RVLM after one systemic injection in conscious rats (66 or 33 mg/kg, i.p.); and 3) compare Mn^{2+} enhancement in the RVLM to other regions to determine an appropriate method of normalization of T_1-weighted images. In our proof-of-concept and proof-of-principle studies, Mn^{2+} was identified by MRI in the rat RVLM after direct microinjection or via retrograde transport following spinal cord injections, respectively. Systemic injections in conscious rats produced significant Mn^{2+} enhancement at 24 hours ($p<0.05$). Injections of 66 mg/kg produced greater enhancement than 33 mg/kg in the RVLM and paraventricular nucleus of the hypothalamus ($p<0.05$ for both), but only when

*Correspondence to: Patrick J. Mueller, Ph.D., Department of Physiology, Wayne State University School of Medicine, 540 E. Canfield, Detroit MI 48201, Phone: 313-577-1559, FAX: 313-577-5494, pmueller@med.wayne.edu.
+Denotes shared first authorship

Conflict of Interest

The authors have no conflicts of interest.

normalized to baseline scans without Mn^{2+} injection. Consistent with findings from our previous functional and anatomical studies demonstrating subregional neuroplasticity, Mn^{2+} enhancement was higher in the rostral regions of the RVLM ($p<0.05$). Along with important technical considerations, our studies support the development of MEMRI as a potential method to examine RVLM activity over time in conscious animal subjects.

Graphical Abstract

MEMRI produced extensive functional and anatomical localization of RVLM, a brain region important in blood pressure regulation. Conscious rats exhibited greater Mn^{2+} enhancement in rostral versus caudal RVLM (*, p=0.004) (A), consistent with increased dendritic branching reported previously (B). With important dose and image normalization considerations, these studies support continued development of MEMRI for examining RVLM activity in conscious subjects. The exciting possibility of longitudinal studies comparing physiological and pathophysiological conditions related to cardiovascular disease is proposed.

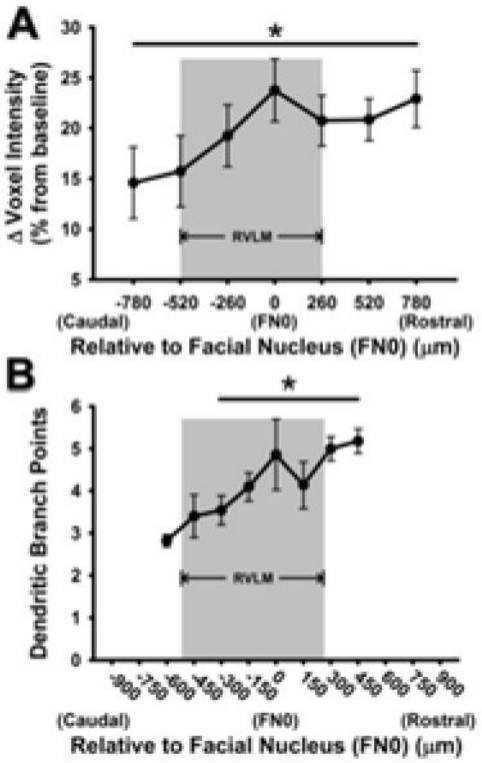

Keywords

imaging; brainstem; neuronal activity; *in vivo*; conscious

Introduction

The rostral ventrolateral medulla (RVLM) is an important brainstem region involved in the maintenance of arterial pressure, via modulation of sympathetic nervous system activity[1]. RVLM neurons project directly to the intermediolateral cell column of the spinal cord and form monosynaptic connections with sympathetic preganglionic nerves[2, 3]. Functional studies support the role of the RVLM in blood pressure regulation as direct activation of RVLM neurons with microinjections of glutamate increases arterial pressure; whereas inhibition of the RVLM produces profound decreases in arterial pressure[4–9]. Although the RVLM is critically important to normal cardiovascular function, it is also implicated in dysregulation of sympathetic nerve activity, increased vascular tone and end-organ damage associated with several cardiovascular disease risk factors including hypertension, heart failure and a sedentary lifestyle[10–13]. Related to the latter, sedentary conditions have also been shown to produce a regionally-dependent neuroplasticity in the RVLM such that more rostrally located neurons exhibit greater dendritic branching and responsiveness to direct excitation by glutamate microinjection[14, 15]. As cardiovascular disease remains the leading cause of death in the United States, it is imperative to understand the central nervous system mechanisms by which these pathophysiological states develop and progress over time[10, 12, 13, 16].

In animal studies, the activity of RVLM neurons has been assessed using techniques developed in both conscious and anesthetized preparations, including single unit recordings[17–20] and Fos immunohistochemistry[21–24]. In humans, blood-oxygen-level dependent (BOLD) imaging has also been recently used to identify tonically active regions of the brainstem, which include the RVLM[25]. However, the use of methods to understand chronic changes in neural activity in conscious subjects are limited to large animals (single unit recordings), cross sectional post-mortem studies (Fos-type), or by methods with indirect inferences of neuronal activity (BOLD). Because of the importance of the RVLM in physiological and pathophysiological changes in blood pressure regulation, there is a critical need to develop complementary strategies which allow for repeated, high spatial resolution measurements of neuronal activity in the RVLM of awake subjects over time. Such techniques would be invaluable in determining the levels of involvement of specific brain regions during the development, progression and end-stage consequences of various cardiovascular diseases.

To address this important need, we have begun investigating the use of manganese-enhanced magnetic resonance imaging (MEMRI), which allows for non-invasive *in vivo* assessment of neuronal activity in the brain[26–29]. With chemical properties similar to those of the divalent ion calcium, Mn^{2+} enters excitable cells and because of its paramagnetic properties, areas with increased accumulation of Mn^{2+} can be visualized using MRI through the shortening of the T_1 relaxation time of protons[30]. The combination of these properties: paramagnetism and activity-dependent accumulation in excitable cells, allows for subsequent detection at very high spatial resolution. Quantitation of Mn^{2+} enhancement also allows for differences in neuronal activity to be detected across experimental groups[24]. Furthermore, since Mn^{2+} can be administered systemically via intraperitoneal or subcutaneous routes to conscious, freely moving animals, the degree of Mn^{2+} uptake occurring over several hours can then be

monitored at later time points via MRI[26, 27, 31]. Lastly, since imaging can be done under acute, recoverable anesthesia, longitudinal studies can be performed on the same groups of animals [27, 32].

MRI is advantageous in part because different acquisition protocols allow for generation of different types of images, including T_1-map and T_1-weighted images, which can be then be used to test for internal consistency of results in the same animal. T_1-weighted images are often normalized because they can vary according to multiple factors such as pulse sequence, coil placement and scanner hardware calibration[26]. In general, previous studies have normalized T_1-weighted voxel intensities to nearby tissue such as muscle [26, 33]. Other studies have performed baseline scans in the absence of Mn^{2+} injection and have reported data as an absolute or percent change from this baseline scan [34–36]. To our knowledge, there has been no systematic analysis within a single study in which different types of normalization have been compared following a single administration of Mn^{2+} under the following conditions: 1) utilizing more than one concentration of Mn^{2+}; 2) repeat scanning over time in a longitudinal fashion, and 3) obtained T_1-map images during each of the scanning session in every animal to provide an additional level of validation.

In this initial study, our goals were to: 1) validate our proof-of-concept and proof-of-principle studies that Mn^{2+} enhancement, via use of MEMRI, could be identified in functionally- and anatomically-localized regions of the RVLM on MRI scans of the rat brainstem; 2) quantify the dose dependency and time course of Mn^{2+} enhancement in the RVLM after one systemic injection in conscious rats (66 or 33 mg/kg, i.p.); and 3) compare Mn^{2+} enhancement in T_1-weighted images of the RVLM to other regions and tissues for the purposes of validating an appropriate method of normalization. We hypothesized that the RVLM would be readily identified on MRI scans of anesthetized animals either following direct microinjection of Mn^{2+} into the RVLM or via retrograde transport of Mn^{2+} following injection into the spinal cord. Based on previous studies, we also hypothesized that following systemic administration, Mn^{2+} uptake would be significant after 24 hours and that a higher dose would produce a significantly greater enhancement. Finally, we hypothesized that different methods of normalization would yield consistent results.

Methods

Ethical statement

All experiments were approved by the Institutional Animal Care and Use Committee of Wayne State University and performed in accordance with the National Academy of Sciences' *Guiding Principles in the Care and Use of Animals* as adopted by American Physiological Society. Male Sprague Dawley rats (Harlan, Indianapolis, IN) were housed in AALAC-accredited facilities with controlled temperature and light (12:12 light:dark cycle). Animals were placed in standard polycarbonate cages and given food (Purina LabDiet 5001: Purina Mills, Richmond, IN) and tap water *ad libitum*.

RVLM $MnCl_2$ microinjection studies

Four rats (421 ± 29 g, 13–23 weeks old) were used for proof-of-concept experiments in which $MnCl_2$ was injected directly into the pressor region of the RVLM in order visualize Mn^{2+} enhancement upon subsequent MRI (see below). Injections of $MnCl_2$ only, were performed post-mortem to ensure that $MnCl_2$ was deposited directly into the RVLM and remained localized in the RVLM without influence of tonic neuronal activity or the possibility of retrograde transport. To this end, rats were anesthetized with Isoflurane (5% induction, followed by 2% maintenance) for RVLM microinjections similar to our previous studies[6, 37]. All rats had the following surgical manipulations performed: femoral arterial and venous catheterization; tracheostomy and placement of an endotracheal tube; splanchnic nerve electrode implantation; and exposure of the brainstem for RVLM microinjections [6, 37]. After positioning the rats in a rodent stereotaxic instrument (Kopf; Tujunga, CA), Inactin was infused (100 mg/kg, i.v.) and isoflurane was withdrawn slowly. Microinjections of glutamate were performed using single barrel glass pipettes drawn to diameters of 10–30 μm. Depending on the type of experiment being performed, different concentrations of glutamate (10 or 100 mM, 30 nl, respectively) were used to identify the pressor region of the RVLM based on expected dose-dependent increases in arterial pressure and sympathetic nerve activity observed in our previous studies [6, 38]. At these concentrations and volumes of glutamate, responses were brief and quickly reversible, lasting approximately 10 seconds in duration, and were not predicted to have any effect on our ability to detect Mn^{2+} in the MRI when $MnCl_2$ was injected post-mortem into the RVLM (see below). Using previously established stereotaxic coordinates[6, 38], pipette tips were placed 3.4–3.8 mm below the dorsal surface of the brain, 0.8–1.2 mm rostral and 1.8–2.2 mm lateral to calamus scriptorius, under visual guidance of a dissecting microscope. Injections were performed using a calibrated reticule on a compound microscope (150X). At the end of the *in vivo* experiments and prior to receiving $MnCl_2$ into the RVLM, animals were euthanized (Fatal-Plus 0.2 ml; Vortech, Dearborn, MI). $MnCl_2$ ($MnCl_2$•$4H_2O$, 1–800 mM, 3–30 nl prepared in 2% Chicago Sky Blue 6B; Sigma-Aldrich, St. Louis, MO) was injected at the same coordinates in which pressor and sympathoexcitatory responses were identified by glutamate injections. As soon as the post-mortem microinjections of $MnCl_2$ were completed, animals were brought to the MRI facility for scanning. The four animals used in this proof-of-principle experiment were initially intended for other *in vivo* experiments, one of which involved sinoaortic denervation 14 days prior to acute microinjection of manganese. By design, microinjections of Mn^{2+} occurred in the post-mortem state, which minimized the possibility that Mn^{2+} spread outside the region of the RVLM which may have occurred in vivo due to movement of CSF, uptake by active neurons or by diffusion into and transport by the cerebral circulation.

Spinal cord injections of $MnCl_2$ and retrograde tracing

To take advantage of the retrograde tracer properties of $MnCl_2$ and to further confirm the region of the RVLM containing bulbospinal neurons on MRI scans, two additional rats (385g and 391g, 14 weeks old) were anesthetized for spinal cord microinjections of $MnCl_2$ using methods above and similar to our previous studies [39–41]. Briefly, rats were anesthetized with isoflurane (5% induction, followed by 2% maintenance) and placed in a stereotaxic frame in order to perform an aseptic laminectomy at T9/T10. Microinjections of

$MnCl_2$ (100 or 800 mM, 30 or 60 nl, respectively; Sigma-Aldrich) were performed into the intermediolateral cell column. Following microinjections, a small piece of gel foam was placed over the spinal cord and muscle. Skin layers were then closed separately with suture and surgical staples, respectively. Animals which received spinal cord injections were allowed to recover for 48 hours. This recovery time allowed for retrograde transport of Mn^{2+} from the spinal cord to the RVLM, and was based on the transport rates of Mn^{2+} (1–3 mm/hr) reported in the literature [42–44].

Systemic injections of $MnCl_2$ in conscious animals

Ten male, Sprague Dawley rats (97 ± 3g upon arrival, 5–6 weeks old at baseline scan) were initially scanned without an injection of $MnCl_2$ to establish baseline signal intensities in the RVLM. To verify that the vehicle for Mn^{2+} preparations (i.e. normal saline) would have no effect on imaging results, we injected four of the ten rats with the same volume of normal saline (0.9%, 2.2 ml/kg, i.p.) that was used during subsequent $MnCl_2$ injections. As with the $MnCl_2$ injections, injections of normal saline were performed 24 hours prior to MRI scanning. Analysis of baseline scans from saline injected and non-injected animals revealed no significant differences in signal intensity (Student t-test, p=0.404). Therefore, individual baseline scans from each animal were used as one form of normalization by calculating the percent change in ROI mean voxel intensity between scans taken before and scans taken after injections of $MnCl_2$. One week after baseline scans, non-injected and saline-injected animals were randomly divided into two groups and a single dose of $MnCl_2$ (33 or 66 mg/kg) was administered by intraperitoneal injection to each group (n= 5 per group, $MnCl_2$ injection equivalent to 167 and 333 mmol/kg, respectively). Based on our previous studies and others, these doses were expected to enhance voxel intensity in brainstem areas near the RVLM without causing detrimental behavioral, electrophysiological or neuroanatomical changes[26, 27, 29, 45, 46]. A single $MnCl_2$ injection was given to each animal 24 hours before the second MRI session. Animals were then scanned weekly for three weeks without additional injections of $MnCl_2$, in order to determine the time course of Mn^{2+} enhancement in multiple regions including the RVLM, PVH, pituitary gland, surrounding muscles, and cerebrospinal fluid (see data analysis below).

MRI scanning

For each imaging session, animals were weighed, anesthetized with isoflurane (5% induction; 2–3% maintenance) and placed in an animal carriage with a heated recirculating water platform to maintain body temperature. The head was stabilized by both a bite bar and the isoflurane nose cone. T_1-weighted localizing MR images were used to ensure that the brain was level and the pituitary gland was centered in each scan. A 2-element phased array, receive-only surface coil for rat brain was placed over the dorsal surface of the rat's head. Scans were performed on a 7T ClinScan system with a Siemens console controlled by the Syngo software (Siemens Corporation, Washington D.C, USA). (For details of imaging methods see Bissig and Berkowitz 2009 [29]; 2011 [47]).

T_1-weighted imaging

A transmit-only whole body coil and receive-only surface coil were used to acquire two types of images based on a turbo-FLASH sequence for T_1-weighted images: Scans acquired

with a slice-selective inversion pulse generated magnetization prepared rapid acquisition gradient echo (MPRAGE) and those without the inversion pulse produced proton density weighted (PDGE) images. MPRAGE and PDGE shared almost all parameters (flip angle of 3°; TE 3.03 ms; NA 1; echo spacing 7.77 ms; matrix size 192×192×112; FOV 2.50 cm × 2.50 cm × 2.91 cm; providing a resolution of 130 μm × 130 μm × 260 μm) and covered the same region of the brain; that is, along the entire rostrocaudal axis of the brain from the spinomedullary junction to the olfactory bulb. MPRAGE imaging took 16 minutes (8 minutes per scan X 2 replicates) and PDGE imaging took approximately 6 minutes (3 minutes per scan X 2 replicates). MPRAGE/PDGE ratio images were created to minimize unwanted influences on signal intensity e.g. distance from the surface coil [48]. Because the PDGE image is essentially free of T_1 weighting [49], the ratio image primarily represents tissue T_1, with higher values within the pre-Mn^{2+} image implying higher endogenous $1/T_1$ (i.e., white > gray matter) and higher values in post- versus pre-Mn^{2+} injection implying greater Mn^{2+} accumulation as in previous work [26, 47].

T_1-mapping

During the same MRI sessions, separate T_1-mapping scans were also performed on each animal. Region of interest (ROI) partial saturation T_1-mapping data were acquired using a dual coil mode on the 7T Bruker Clinscan system: several multiple spin-echo images (TE=11 ms, Turbo factor=9, Echo Spacing=10.9 ms, four averages, 20 × 20 mm^2, matrix size 192 × 192, resolution 104 μm) were acquired at different repetition times (TRs) in the following order (number of repetitions for each TR is given in between parentheses): 0.15 seconds (6), 3.50 seconds (1), 1.00 seconds (2), 1.90 seconds (1), 0.35 seconds (4), 2.70 seconds (1), 0.25 seconds (5) and 0.50 seconds (3). To compensate for reduced signal-noise ratios at shorter TRs, progressively more images (higher number of repetitions) were collected as the TR decreased [47]. Each imaging session was approximately 15 minutes which allowed acquisition of 23 total images used in the construction of the final T_1-map for each scan. Two T_1-Map scans were performed to acquire two 400 μm slices that were designated as rostral and caudal RVLM by their common origin at the caudal pole of the facial nucleus.

The combination of T_1-weighted scan time (~30 minutes) and T_1-mapping scan time (2 X 15 minutes) resulted in a total imaging time for each animal of approximately one hour. At the end of each imaging session, rats were removed from the MRI and animal carriage, placed on a heating pad and allowed to regain consciousness. Sternal recumbency was used to assess consciousness and once animals were fully conscious they were returned to their home cage.

Image processing

Image processing of whole brain scans was performed according to our previous study [26]. Briefly, we used in-house developed R language scripts (v.2.9.0; R Development Core Team (2009); http://www.R-project.org) to provide 130 μm isotropic voxels for later processing instead of the original 130 μm x130 μm x 260 μm voxel dimensions. For each subject at each time point, the two summed MPRAGE images were divided by the two summed PDGE images on a voxel-by-voxel basis to produce the T_1-weighted ratio images.

T_1-mapping images were processed as follows: single images acquired with the same TR were first registered (rigid body) and then averaged. These averaged images were then registered across TRs. ROIs were analyzed by calculating $1/T_1$ maps by first fitting to a three-parameter T_1 equation (y=a + b*(exp(-c*TR)), where a, b and c are fitted parameters) on a pixel-by-pixel basis using R (v.2.9.0, R Development Core Team [2009]. R: A language and environment for statistical computing. R Foundation for Statistical Computing, Vienna, Austria. ISBN 3–900051–07–0) scripts developed in-house and the minpack.lm package (v. 1.1.1, Timur V. Elzhov and Katharine M. Mullen minpack.lm: R interface to the Levenberg-Marquardt nonlinear least-squares algorithm found in MINPACK. R package version 1.1–1.). The reciprocal ($1/T_1$) values were then assessed within defined ROIs using ImageJ (see below) and directly reflect Mn^{2+} levels[47].

Defining ROIs

ROIs were manually drawn onto each image acquired to quantify Mn^{2+} enhancement similar to previous studies [26, 50]. For the RVLM, ROIs were initially conceptualized using a combination of information provided by the direct microinjection proof-of-concept studies (Figure 1); the proof-of-principle studies using retrograde tracing (Figure 2); and traditional anatomical landmarks provided in a standard rat atlas[51] and previous anatomical studies performed by our laboratory and others[1, 12, 14, 41, 51]. For the PVH, identification was done similarly, using traditional landmarks around the base of the third ventricle; caudal to the anterior commissure; the rat atlas [51]; and anatomical studies from our laboratory and others [52–55]. From these images we obtained voxel intensities in multiple regions including the RVLM, PVH, pituitary gland, surrounding muscles, and cerebrospinal fluid. Based on our previous studies of subregional variation [14, 15], the RVLM was further divided into caudal and rostral subregions using the caudal pole of the facial nucleus as a reference landmark distinguishing between caudal and rostral regions. The RVLM and PVH as well as corresponding areas of muscle and cerebrospinal fluid were determined bilaterally.

To determine the effect of different types of normalization used in previous studies for other brain regions, we established ROIs for a tissue type other than brain (i.e. muscle), and for a region in which Mn^{2+} uptake was expected to be minimal at the time of the first scan (i.e. cerebrospinal fluid at 24 hours). For the RVLM, two different muscle groups were analyzed in order to account for similar dorsoventral and mediolateral locations relative to the RVLM. The cleidomastoid was located laterally at the same dorsal ventral position relative to the RVLM and the splenius muscle was located dorsally to the RVLM at the same mediolateral location relative to the RVLM. For the PVH, ROIs were obtained from the temporalis muscle, located at a similar dorsoventral depth on the same scans of the PVH. ROIs were also obtained from cerebrospinal fluid (CSF) located at the level of the RVLM (bilaterally) as well as from the cerebral aqueduct which was readily identifiable in all scans.

Mn^{2+} enhancement in the pituitary gland has been used as a positive control in previous studies from our laboratory [26, 27]. We used ROIs taken from the pituitary to determine the effectiveness of our i.p. injections in the present study. The pituitary was identified in both coronal and sagittal views of T_1-weighted images. ROIs were drawn in both the dorsoventral and rostrocaudal planes by switching back and forth between the sagittal and coronal views.

ROIs of the pituitary were completed in the mediolateral plane by utilizing the coronal view of each section. One ROI was used to estimate Mn^{2+} enhancement of the pituitary in each scan of every animal.

Image analysis

For analysis of T_1-weighted images, manually drawn ROIs described above were placed on images using MRIcro v.1.40 [56]. ROI mean voxel intensities were obtained bilaterally within MRIcro using seven consecutive (for RVLM) and eight consecutive (for PVH) coronal slices along the rostrocaudal extent of the brain. For muscle normalization, ROI mean voxel intensities of the left and right RVLM and PVH were normalized to their respective lateral (cleidomastoid) and dorsal (splenius) for the RVLM and the temporalis muscle region for the PVH by the following formula: [Region of Interest Signal Intensity (ROI SI) = RVLM SI/Muscle SI *100]. Values from left and right sides were then averaged and reported as a single value for each slice. Mn^{2+} enhancement in RVLM and PVH were determined in two ways: 1) Individual 260 μm slices at each level of the RVLM (7 slices total) and PVH (8 slices total) were averaged across animals and compared to determine sub-regional variation. 2) Measures of total RVLM neuronal activity were estimated by averaging ROIs from four consecutive coronal slices (260 μm) which were taken caudal (2 slices) and rostral (2 slices) to the caudal pole of the facial nucleus. These boundaries were chosen based on previous studies from our laboratory and others that have defined the rostrocaudal location of bulbospinal catecholaminergic and non-catecholaminergic RVLM neurons [1, 39, 41]. ROI mean voxel intensities from T_1-weighted images of Mn^{2+} injected animals were normalized as percent change from the voxel intensity of baseline (i.e. non-Mn^{2+} injected) scan or using voxel intensities from the corresponding muscle regions for each brain area. For the pituitary gland, mean voxel intensities were created from each animal's ROI and expressed in absolute terms to serve as a positive confirmation of Mn^{2+} uptake following i.p. injections.

For analysis of T_1-mapping images taken of the RVLM only, ROIs were created based on the same criteria used for T_1-weighted image and were analyzed in ImageJ. Voxel intensities representing absolute Mn^{2+} enhancement ($1/T_1$ values) were obtained via custom ImageJ scripts used in our previous studies [57]. Left and right $1/T_1$ values were averaged for mean Mn^{2+} enhancement in both the left and right RVLM. ROI mean voxel intensities from T_1-mapping images were expressed in absolute terms ($1/T_1$ ratio).

Statistics

All data were analyzed using SigmaStat Version 3.5 (Systat Software, San Jose, CA). One and two way repeated measures analyses of variance were used and when significant interactions occurred, posthoc multiple comparisons tests (Holm-Sidak) were performed for further interpretation of the data. A standard two-tailed Student's t-test was used to asses potential differences between baseline values of saline injected versus non-injected signal intensities. Data were considered statistically significant if p values were less than 0.05. All data are expressed as mean ± standard error of the mean.

Results

Proof-of-concept microinjection studies

Consistent with previous studies[6, 58], *in vivo* microinjections of glutamate (10 or 100 mM, 30 nl) produced prompt and significant increases in arterial pressure (Δ 17±2 mmHg, n=4). Following post-mortem microinjections of $MnCl_2$ at the same coordinates that produced the pressor responses, subsequent MRI scanning revealed prominent Mn^{2+} enhancement along the rostrocaudal axis of the ventrolateral medulla very similar to our previous studies using dye microinjections to identify injection sites[6, 58]. Figure 1 contains a set of rostrocaudal T_1-weighted images from an individual animal which was injected with $MnCl_2$ into the RVLM in the post-mortem state. In this case, as with other similar volumes and concentrations, 15 nl of 400 mM $MnCl_2$ administered into the RVLM increased voxel intensity. ROI mean voxel intensity peaked near the ventral aspect of the caudal pole of the facial nucleus, the anatomical landmark classically used to define the RVLM [1]. Figure 1 also demonstrates the utility of matching T_1-weighted images taken in series (left) with those in a standard rat atlas (right)[51]. In this case, Mn^{2+} enhancement was greatest at −12.12 mm from Bregma and diminished in both rostral and caudal directions in a fairly symmetrical pattern, consistent with the anatomically defined region of the RVLM. Similar results were found in the other animals with direct post-mortem microinjections of Mn^{2+}. Decreasing ROI mean voxel intensities were observed at lower concentrations (1–100 mM) and volumes (3–15 nl; data not shown).

Proof-of-principle spinal cord injection studies

As shown in Figure 2, injection of $MnCl_2$ (60 nl, 800 mM) into T9/T10 of the spinal cord resulted in an increase in voxel intensity in the region of the brainstem consistent with the location of one subset of bulbospinal barosensitive neurons, which are known to project to the T9/T10 region. The pattern and distribution of Mn^{2+} enhancement was very similar to that produced in our previous studies in which we injected different retrograde tracers at this same level of the spinal cord [39–41]. As similarly identified by the glutamate injections in our proof-of-concept studies, this area corresponds to that previously described as the RVLM; that is, the region located ventral to the nucleus ambiguus, lateral to the pyramidal tracts and medial to the spinotrigeminal tract [1, 12].

Systemic injections of $MnCl_2$ in conscious animals

The use of anesthesia in proof-of-concept and proof-of-principle studies limited our interpretations of both studies, but allowed us to clearly define and confirm the location of the RVLM in our studies in conscious animals. Body weights obtained during the protocol are shown in Table 1. Rats in each group (33 mg/kg and 66 mg/kg) gained weight at typical rates (30–40 g/week) for animals of this age and strain. A slight decrease in body weight (6 and 8%) tended to be observed in 33 mg/kg and 66 mg/kg groups, respectively, 24 hours after injection of $MnCl_2$; but did not reach significance via two way RM ANOVA. Increases in body weight from Day 1 to Day 8 did appear similar to or greater than that occurring the week prior to $MnCl_2$ injection, suggesting there were no prolonged effects of the single dose of $MnCl_2$ on body weight. Lastly, there was no main effect of dose on body weights over the course of the study ($p>0.05$, Two way RM ANOVA; Table 1).

T_1-weighted Imaging

RVLM—A representative T_1-weighted image and corresponding ROI for the RVLM is shown in Figure 3A. Figure 3B demonstrates the time course of results of repeated T_1-weighted scanning of animals at each post-injection time point and are expressed as percent change to normalize to non-Mn^{2+} injected baseline scans in each animal. Similar to T_1-map scanning (see below), single injections of 33 or 66 mg/kg increased ROI mean voxel intensities at the initial scan of 24 hours and decreased thereafter over time (Figure 3B). Also, similar to T_1-map scanning, there was a significantly greater change in animals injected with 66 mg/kg compared to animals injected with 33 mg/kg $MnCl_2$ (Figure 3B).

T_1-weighted imaging also afforded us the opportunity to analyze Mn^{2+} enhancement along the rostrocaudal axis of the ventrolateral medulla using percent change in each 260 μm scan relative to its non-Mn^{2+} injected baseline scan. This analysis in animals injected with 66 mg/kg $MnCl_2$ revealed a pattern of increased signal intensity in the more rostral regions of the RVLM, compared to the more caudal portions ($p<0.05$, main effect, Figure 4A). Interestingly, these results bear a striking similarity to our previous study examining a pattern of increased dendritic branching in more rostral regions of the RVLM from sedentary rats (replotted in Figure 4B). We speculate the pattern of increasing caudal to rostral signal intensity was not observed in animals injected with 33 mg/kg $MnCl_2$ because of a lower contrast-to-noise ratio (data not shown).

PVH—Figure 5 represents a T_1-weighted scan of the PVH (Figure 5A), obtained during the same scanning sessions for the RVLM, as well as the time course of Mn^{2+} enhancement as a percent of each animal's baseline scan (Figure 5B). Similar to the RVLM, when PVH scans were normalized to their respective baseline scans, there was a significant effect of time and dose for Mn^{2+} enhancement. ROI mean voxel intensities decreased to levels not significantly different from baseline intensity after 22 days ($p<0.05$).

RVLM versus PVH—We directly compared Mn^{2+} enhancement in the RVLM and PVH to understand how Mn^{2+} enhancement occurs in different brain regions involved in cardiovascular regulation. As mentioned above separately, both regions exhibited significant main effects of dose and time with similar patterns of increased enhancement at 1 and 8 days and the higher 66 mg/kg dose producing greater levels of enhancement compared to the 33 mg/kg dose. On a percent basis, 66 mg/kg produced a 21±3% increase in enhancement relative to baseline in the RVLM at 24 hours, whereas the same dose produced a 26±3% enhancement relative to baseline in the PVH after 24 hours. In contrast, 24 hours after the 33 mg/kg injections, the RVLM appeared to have a lower level of Mn^{2+} enhancement (8±1%) compared to PVH (17±1%).

Pituitary gland—$MnCl_2$ produced significant increases in absolute voxel intensity in T_1-weighted images of the pituitary gland (Table 2) and allowed secondary verification that our i.p. $MnCl_2$ injections produced robust levels of enhancement as would be expected in each animal. As with T_1-map results of the RVLM, absolute voxel intensities measured in T1-weighted scans in the pituitary gland were highest at 24 hours, significantly higher for 66 vs 33 mg/kg and diminished gradually over time (Table 2).

Cerebrospinal Fluid—We examined regions containing cerebrospinal fluid in each slice containing the RVLM as well as in the cerebral aqueduct which was readily identifiable in MRI scans from all animals. There were no significant differences in ROI mean voxel intensity at 24 hours or 8, 15, or 22 days following 66mg/kg of $MnCl_2$ compared to non-$MnCl_2$ injected baseline values in regions of cerebrospinal fluid in scans of the RVLM or the cerebral aqueduct (Table 3). These data suggest that Mn^{2+} was cleared from the cerebrospinal fluid of our animals within 24 hours at either dose, consistent with reports from previous studies.

Muscle tissues used for normalization—Figure 6A indicates representative ROIs for both the lateral muscle group (i.e. cleidomastoid) and dorsal muscle group (i.e. splenius). In the lateral muscle group, injection of Mn^{2+} showed no main effect of time or effect of dose ($p>0.05$ for both and no interaction) when expressed as a percent change relative to non-Mn^{2+} injected baseline scans (Figure 6B). In contrast, Mn^{2+} enhancement increased significantly in the dorsal muscle group and a main effect of time when expressed as a percent change relative to non-Mn^{2+} injected baseline scans (Figure 6C). However, similar to the lateral muscle group, there was no significant effect of dose on Mn^{2+} enhancement in the dorsal muscle group ($p>0.05$).

Normalization of T_1-weighted Scans of RVLM and PVH to Neighboring Muscle Tissue

RVLM—Figure 7A and 7B demonstrates the effects of normalizing Mn^{2+} enhancement in the RVLM to lateral and dorsal muscle tissue. Normalizing RVLM ROI mean voxel intensities to the lateral muscle region resulted in no significant effect of time or dose (Figure 7A). Similarly, normalization of RVLM ROI mean voxel intensities to the dorsal muscle region resulted in no significant effect of dose but did result in a significant main effect of time (Figure 7B) and suggested a slight but significant increase in Mn^{2+} enhancement over time independent of dose.

PVH—Normalization of PVH scans to the nearby temporalis muscle demonstrated a signal intensity pattern was elevated at 24 hours post injection compared to non-injection control at Day −7. Interestingly, ROI mean voxel intensity continued to increase after 24 hours, reaching peak values at 8 and 15 days for 66 and 33mg/kg doses, respectively (Figure 7C).

T_1-Map Imaging

Figure 8A demonstrates a representative image using T_1-mapping in a 400 μm slice of the rat brainstem taken at the level of the RVLM. Figure 8B illustrates the time course of results obtained at the five study time points including the non-$MnCl_2$ injected baseline scan (Day −7) and at 1, 8, 15 and 22 days after injections of 33 or 66 mg/kg injection. There were significant main effects of time and dose for the $1/T_1$ ratio when examined by two-way RM ANOVA, suggesting increases in Mn^{2+} enhancement in the RVLM that was greater following injection of 66 mg/kg vs. 33 mg/kg $MnCl_2$. The results showed that 1/T1 varied at baseline between 0.62±0.03 and 0.67±0.03 and reached a maximum between 0.72±0.03 and 0.82±0.04 at 24 hours for injections of 33 and 66 mg/kg injections, respectively. A significant interaction between dose and time allowed for post hoc testing which revealed significant increases in Mn^{2+} enhancement one day after $MnCl_2$ injection compared to the

non-$MnCl_2$ injected baseline scan for both doses (Figure 8B). Injections of 66 mg/kg $MnCl_2$ produced greater Mn^{2+} enhancement compared to injections of 33 mg/kg $MnCl_2$ at both one and eight days following $MnCl_2$ injection (Figure 8B).

Discussion

The most important and novel findings of this study are that: 1) The rostral region of the ventrolateral portion of the medulla containing tonically active, bulbospinal neurons is readily identified in MRI images immediately following direct injection of $MnCl_2$ into the RVLM or via retrograde transport from injections performed in the spinal cord of rats two days prior to MRI. 2) Systemic injections of $MnCl_2$ produced signal intensities in the RVLM that were significantly elevated at 24 hours compared to baseline non-Mn^{2+} injected scans. 3) Signal intensities were dose-related with 66 mg/kg $MnCl_2$ producing significantly greater enhancement than 33 mg/kg. 4) Normalization of T_1-weighted scans to muscle tissue from the same scans used to generate data from the RVLM or the PVH did not consistently result in predicted time- or dose-dependent effects compared to when data were simply normalized to baseline, non-Mn^{2+} injected scans. RVLM data normalized to baseline scans produced similar results to RVLM data generated from scans using T_1-mapping, the latter of which was performed in every animal at the same time points. 5) Finally, and most intriguing to us, serial slice examination (260 μm/slice) provided by T_1-weighted imaging allowed us to report significantly greater Mn^{2+} enhancement in more rostral subregions of the RVLM. These exciting findings lead us to speculate that enhanced dendritic branching and glutamate sensitivity observed in more rostral regions of the RVLM reported in our previous study[15, 39] may translate into increases in neuronal activity in the same subregions of the RVLM reported here. These developmental studies support the continued exploration of MEMRI as a promising tool for examining the RVLM and other cardiovascular-related brain regions, with advantages in the use of both T_1-weighted and T_1-mapping imaging modalities.

One of the more novel findings from this study was the differential pattern of Mn^{2+} enhancement within sub-regions of the RVLM; that is, ROI mean voxel intensities were significantly greater in the more rostral compared to caudal regions of the RVLM (Figure 4). The enhanced branching in our previous study was reported specifically for bulbospinal, catecholaminergic neurons and in a pattern with a striking similarity to the increased ROI mean voxel intensity in T_1-weighted images of the current study [39]. Given that the rats in the present study were not exercised, and therefore fairly similar to the sedentary rats in our previous study, it is tempting to speculate that our current results provide a functional correlate to the structural plasticity observed in our previous study [39]. They also corroborate our more recent finding of enhanced resting splanchnic sympathetic nerve activity as well as augmented responses to direct stimulation of more rostral regions of the RVLM in sedentary but not physically active rat [15]. We contend that increased dendritic arborization likely promotes enhanced resting neuronal activity and reactivity to glutamate in more rostral regions of the RVLM, resulting in enhanced resting and stimulated sympathetic nerve activity reported in our previous studies [6, 37]. Certainly confirmation of these speculations require direct comparison of Mn^{2+} enhancement in the RVLM of sedentary versus physically active animals, studies which are currently ongoing in our laboratory.

Since to our knowledge this is the first report to provide MRI data from the RVLM of conscious rats, it was important for us to validate that the anatomy of the RVLM was properly demarcated by ROIs, which did not vary over time in the present study. We confirmed this in several ways, using both proof-of-concept and proof-of-principle studies. First, we performed a proof-of-concept study to ensure that conditions existed in which $MnCl_2$ affected the relaxation rate of RVLM tissue within the region that contained neurons involved in blood pressure regulation. We did so by injecting $MnCl_2$ directly into sites pre-identified *in vivo* via well-established microinjection techniques used in several our previous studies [6, 37, 59]. Injections of $MnCl_2$ were performed post-mortem to ensure that $MnCl_2$ was deposited directly into the RVLM and remained localized in the RVLM without influence of tonic neuronal activity or the possibility of retrograde transport. Post-mortem microinjections of $MnCl_2$ produced MRI enhancement patterns across the rostrocaudal axis very similar to those produced by dye injections used to demarcate glutamate injection sites in our previous studies [6, 37, 59]. Injections of $MnCl_2$ in the post-mortem condition would likely influence T_1 relaxation due to the reduction in body temperature; however, since the experiment was anatomical not functional, the drop in body temperature did not negate our ability to locate enhancement on MRI scans. The experiments provided conceptual proof that when present at sufficient concentrations, $MnCl_2$ affects the relaxation rate of the RVLM tissue and could be detected in the RVLM upon subsequent MRI.

Our proof-of-principle studies took advantage of the tract tracing properties of Mn^{2+} [42, 60] by injecting it into the intermediolateral cell column of the spinal cord, where bulbospinal RVLM neurons are known to terminate upon sympathetic preganglionic neurons [39–41]. As shown in Figure 2, following a 48 hour period for retrograde transit time, MRI scanning resulted in the classic oval shaped pattern of Mn^{2+} enhancement within the RVLM. Although a variety of shapes have been used to demarcate the shape of the RVLM, this pattern of Mn^{2+} enhancement was remarkably similar to that reported previously by us and others in studies of bulbospinal RVLM neurons using immunohistochemical and immunofluorescent staining techniques in combination with tract tracers[1, 12, 14, 41, 51]. These proof-of-principle studies provided evidence that when sufficient quantities of $MnCl_2$ were taken up by active spinally-projecting neurons of the RVLM, we were able to visualize Mn^{2+} enhancement upon subsequent MRI scanning. Thus, the results of both proof-of-concept (brainstem microinjection) and proof-of-principle (spinal cord microinjection) experiments were in good agreement and allowed us to visualize the location of the RVLM within the context of traditional and non-traditional landmarks in MRI images aided additionally by comparisons with a standardized rat atlas [51].

One of the main strengths of studies utilizing MEMRI has been the ability to repeatedly image the same animals over time allowing for longitudinally-based studies. However, previous studies examining Mn^{2+} enhancement over time in other brain regions have shown that temporal patterns may be particular to specific brain regions and are likely dependent on the properties of the region itself [61–64]. Thus, establishing a time course of Mn^{2+} enhancement in the RVLM following a single injection in conscious animals was important for two reasons: 1) it allowed for selection of an appropriate time course for imaging the RVLM following systemic injections and 2) it established the necessary amount of time required between injections of $MnCl_2$ when a reinjection protocol is warranted for a

longitudinal-type study design. The results of the present study suggest that Mn^{2+} enhancement in the RVLM returns to levels not significantly different from baseline by day 15 post-injection even when a higher dose such as 66 mg/kg is used. These findings are consistent with previous studies examining Mn^{2+} enhancement levels in other brain regions, which have demonstrated a decrease in signal enhancement over the course of 2–3 weeks [62, 63]. Furthermore, previous studies reported that 99% of $MnCl_2$ is eliminated in feces within five days [65, 66]. Thus, we recommend that future longitudinal studies examining neuronal activity in the RVLM and utilizing multiple time points of analysis wait a minimum of two weeks in between systemic injections to ensure Mn^{2+} levels have returned to baseline levels in the RVLM.

As mentioned above, another main objective of this study was to test two different concentrations of $MnCl_2$ for use in future studies examining neuroplasticity under different physiological and pathophysiological states. We considered that a concentration of $MnCl_2$ would be deemed effective for longitudinal studies if it 1) produced elevated signal intensities within the anatomically defined region of the RVLM following systemic injections and 2) returned to baseline levels within a reasonable time to permit additional injections and scanning over the time course of a study. Following this rationale, larger concentrations of $MnCl_2$ would not necessarily be conducive for longitudinal studies if they produced a delayed return to baseline. As hypothesized, injections of 66 mg/kg $MnCl_2$ produced greater ROI mean voxel intensities when compared to 33 mg/kg in both T_1-weighted and T_1-mapping images, respectively. Animals injected with 33 mg/kg showed increased Mn^{2+} enhancement at 24hrs with T_1-mapping (>10% relative to baseline), but not as much of an increase in ROI mean voxel intensity on a relative basis with T_1-weighted scanning (<10% relative to baseline). We believe these results reflect the quantification process used for the individual types of images collected and that the variability and signal-to-noise in T_1-weighted voxel intensities may have limited our ability to observe equivalent increases in Mn^{2+} after the 33 mg/kg dose. In either case, when normalized to baseline scans (see below), our results are consistent with other studies showing a dose dependent increase in Mn^{2+} uptake in multiple regions in the brain [67, 68] and favor the use of 66 mg/kg over 33 mg/kg to produce a more consistent signal enhancement in the RVLM to discern differences between experimental groups. It is also worth mentioning that in the present study, there was a slight but insignificant decrease in mean body weight 24 hours after $MnCl_2$ injections at both doses (Table 1). This effect was transient and the animals regained their original weight within a few days. The doses in the current study were chosen because they have been considered non-toxic based on the lack of significant changes in normal behavior, electrophysiology or neuroanatomy reported in studies utilizing systemic administration [26, 27, 29, 45, 46]. We recommend careful consideration of dose as well as potential transient effects of $MnCl_2$ administration when interpreting results.

An important issue in using T_1-weighted scanning techniques is the common practice of normalization[26,69]. Because we performed scans in the absence of Mn^{2+} injection, we were able to compare normalization of T_1-weighted images for both the RVLM and PVH to a baseline scan as well as to surrounding muscle tissue. For the RVLM, we normalized separately to two different muscle groups based on their similar dorsoventral or mediolateral locations relative to RVLM. Even with these considerations taken into account, there were

no consistent effects of time or dose that were analogous with the time course observed in the T_1-mapping studies or when data were normalized to baseline scan. Normalizing the RVLM to baseline scans produced results that were nearly identical to similarly timed but separately obtained T_1-mapping results. We found also similar results for the PVH; that is, when normalizing to baseline scans signal intensity increased significantly at 24 hours followed by a predictable decline over the remaining course of the experiment. Again, similar to RVLM, normalization of the PVH to a nearby muscle group exhibited a slight but significant increase in signal intensity at 8 or 15 days, depending on the dose administered. Thus, although normalization of the RVLM and PVH to their respective muscle groups likely reflects different patterns of Mn^{2+} enhancement in brain versus muscle tissue, the results of the present study support performing and normalizing to non-injected baseline scans, when possible. Lastly, to control for potential variation in the MRI scanner over time, we quantified Mn^{2+} enhancement of cerebrospinal fluid in two locations, one in the same scans of the RVLM and the other in the cerebral aqueduct, which was readily identifiable in every animal. Neither cerebrospinal fluid measurements showed a significant increase in Mn^{2+} enhancement at 24 hours or variation at any other time point when compared to baseline values. These data suggests that cerebrospinal fluid may serve as an appropriate time-based control under circumstances where it is cost prohibitive or otherwise impractical to perform a longitudinal study that includes a non-Mn^{2+} injected control group.

Alternatively, T_1-mapping images do not depend on normalization to surrounding tissue to correct for, for example, B1 inhomogeneities and thus are more representative of absolute Mn^{2+} concentration compared to T_1-weighted images [27, 29, 62]. The manner in which T1-weighted imaging was used in this particular study did allow for rostrocaudal analysis (260 μm slices), in addition to allowing us to examine whether other brain regions (PVH; pituitary) and different tissue (muscle) and fluids (CSF) could be used for normalization. Although T1 map imaging was used only for validation purposes in this study, it can also be configured to produce serial slicing of the brain. However, the reduced time, effort and expense of T1 weighted imaging may be a reasonable alternative for studying the RVLM and perhaps PVH.

In summary, it is well known that increased sympathetic outflow is a major risk factor for the development of cardiovascular diseases such as hypertension and chronic heart failure[70]. Evidence from the current study is intriguing in that it suggests that increased neuronal activity in subregions of the RVLM are consistent with the structural and functional neuroplasticity we have reported in previous studies of the RVLM following sedentary conditions[15, 39]. However, and importantly, the time frame and mechanisms by which neuroplasticity occurs in sedentary versus physically active animals develops are unclear. In other words, whether sedentary conditions increase dendritic branching/neuronal activity, chronic exercise decreases dendritic branching/neuronal activity, or if both occur to produce the relative difference between the groups is currently unknown. The benefit of longitudinal MEMRI studies would be that neuronal activity can be measured at multiple time points within the same animal. The results of this study support performing non-injected baseline scans, when possible, due to their usefulness in predicting timelines similar to that observed in T1 map images. This similarity was not observed when using two different muscle groups at similar mediolateral or dorsoventral positions to attempt normalization. Based on the

results of the current study, we also conclude that future studies could utilize multiple systemic injections, a minimum of two weeks apart, and may provide *in vivo* assessments of Mn^{2+} enhancement linked to alterations in neuronal activity due to sedentary conditions, physically active conditions or both.

Acknowledgments

The authors would like to thank Toni Azar, Maryetta Dombrowski, Maxwell Laws, Benjamin Maynard, Melanie Radtke and Christina Wong from Dr. Mueller's laboratory for technical support. We also thank Dr. Yimin Shen from the Wayne State University Small Animal Imaging Core for technical support and expertise with the small animal 7T magnet. We thank the Neural Control of Cardiorespiratory Function Group at Wayne State University School of Medicine for their input during the development of this project and David Bissig for helpful comments on the manuscript. This work was supported by grants from the National Institutes of Health (R01HL096787-05 to PJM); the American Heart Association (AHA25810010 to PJM and AHA PRE25700308 to DJH); the National Institutes of Health Animal Models of Diabetic Complications Consortium and Mouse Metabolic Phenotyping Centers Pilot and Feasibility Programs (BAB), the National Eye Institute (R21 EY021619; R01 EY026584, BAB) and an unrestricted grant from Research to Prevent Blindness (Kresge Eye Institute, BAB); the U.S. Department of Veterans Affairs, Award Number (1I01RX001095-01 to AGH). The content is solely the responsibility of the authors and does not necessarily represent the official views of the National Institutes of Health.

Abbreviations

BOLD	blood-oxygen-level dependent
CSF	cerebrospinal fluid
Mn^{2+}	Manganese
$MnCl_2$	manganese chloride
MEMRI	manganese-enhanced magnetic resonance imaging
MPRAGE	magnetization prepared rapid acquisition gradient echo
NA	nucleus ambiguus
Pfl	paraflocculus
PVH	paraventricular nucleus of the hypothalamus
PDGE	proton density gradient echo
Py	pyramidal tract
ROI	Region of interest
RVLM	rostral ventrolateral medulla
Sp5	spinal trigeminal tract
7	facial nucleus

References

1. Schreihofer, AM., Sved, AF. The ventrolateral medulla and sympathetic regulation of arterial pressure. In: Llewellyn-Smith, IJ., Verberne, AJM., editors. Autonomic control of cardiovascular function. 2. New York: Oxford University Press; 2011. p. 78-97.

2. Dampney RAL. Functional organization of central pathways regulating the cardiovascular system. Physiol Rev. 1994; 74:323–364. [PubMed: 8171117]

3. Zagon A, Smith AD. Monosynaptic projections from the rostral ventrolateral medulla oblongata to identified sympathetic preganglionic neurons. Neuroscience. 1993; 54(3):729–743. [PubMed: 8332259]

4. Ito S, Sved AF. Tonic glutamate-mediated control of rostral ventrolateral medulla and sympathetic vasomotor tone. Am J Physiol. 1997; 273:R487–R494. [PubMed: 9277530]

5. Ross CA, Ruggiero DA, Park DH, Joh TH, Sved AF, Fernandex-Pardal J, Saavedra JM, Reis DJ. Tonic vasomotor control by the rostal ventrolateral medulla: effect of electrical or chemical stimulation of the area containing C1 adrenaline neurons on arterial pressure, heart rate, and plasma catecholamines and vasopressin. J Neurosci. 1984; 4(2):474–494. [PubMed: 6699683]

6. Mischel NA, Mueller PJ. (In)activity-dependent alterations in resting and reflex control of splanchnic sympathetic nerve activity. J Appl Physiol. 2011; 111(6):1854–1862. [PubMed: 21979802]

7. McAllen RM, Dampney RA. Vasomotor neurons in the rostral ventrolateral medulla are organized topographically with respect to type of vascular bed but not body region. Neurosci Lett. 1990; 110(1–2):91–96. [PubMed: 1970144]

8. Adams JM, Madden CJ, Sved AF, Stocker SD. Increased dietary salt enhances sympathoexcitatory and sympathoinhibitory responses from the rostral ventrolateral medulla. Hypertension. 2007; 50(2):354–359. [PubMed: 17592069]

9. Schreihofer AM, Stornetta RL, Guyenet PG. Regulation of sympathetic tone and arterial pressure by rostral ventrolateral medulla after depletion of C1 cells in rat. J Physiol. 2000; 529(Pt 1):221–236. [PubMed: 11080264]

10. Sved AF, Ito S, Sved JC. Brainstem mechanisms of hypertension: role of the rostral ventrolateral medulla. Curr Hypertens Rep. 2003; 5:262–268. [PubMed: 12724060]

11. Wang WZ, Gao L, Wang HJ, Zucker IH, Wang W. Tonic glutamatergic input in the rostral ventrolateral medulla is increased in rats with chronic heart failure. Hypertension. 2009; 53(2): 370–374. [PubMed: 19029485]

12. Guyenet PG. The sympathetic control of blood pressure. Nat Rev Neurosci. 2006; 7:335–346. [PubMed: 16760914]

13. Mueller PJ. Physical (in)activity-dependent alterations at the rostral ventrolateral medulla: influence on sympathetic nervous system regulation. Am J Physiol Regul Integr Comp Physiol. 2010; 298(6):R1468–R1474. [PubMed: 20357021]

14. Mischel NA, Llewellyn-Smith IJ, Mueller PJ. Physical (in)activity-dependent structural plasticity in bulbospinal catecholaminergic neurons of rat rostral ventrolateral medulla. J Comp Neurol. 2014; 522(3):499–513. [PubMed: 24114875]

15. Subramanian M, Mueller PJ. Altered Differential Control of Sympathetic Outflow Following Sedentary Conditions: Role of Subregional Neuroplasticity in the RVLM. Front Physiol. 2016; 7:290. [PubMed: 27486405]

16. Osborn JW, Kuroki MT. Sympathetic signatures of cardiovascular disease: a blueprint for development of targeted sympathetic ablation therapies. Hypertension. 2012; 59(3):545–547. [PubMed: 22311900]

17. Schreihofer AM, Guyenet PG. Identification of C1 presympathetic neurons in rat rostral ventrolateral medulla by juxtacellular labeling *in vivo*. J Comp Neurol. 1997; 387:524–536. [PubMed: 9373011]

18. Guyenet PG, Haselton JR, Sun M-K. Sympathoexcitatory neurons of the rostroventrolateral medulla and the origin of the sympathetic vasomotor tone. Prog Brain Res. 1989; 81:105–116. [PubMed: 2616776]

19. Barman SM, Sugiyama Y, Suzuki T, Cotter LA, DeStefino VJ, Reighard DA, Cass SP, Yates BJ. Rhythmic activity of neurons in the rostral ventrolateral medulla of conscious cats: effect of removal of vestibular inputs. Am J Physiol Regul Integr Comp Physiol. 2011; 301(4):R937–R946. [PubMed: 21734018]

20. DeStefino VJ, Reighard DA, Sugiyama Y, Suzuki T, Cotter LA, Larson MG, Gandhi NJ, Barman SM, Yates BJ. Responses of neurons in the rostral ventrolateral medulla to whole body rotations:

comparisons in decerebrate and conscious cats. J Appl Physiol (1985). 2011; 110(6):1699–1707. [PubMed: 21493724]

21. Li Y-W, Dampney RAL. Expression of c-fos protein in the medulla oblongata of conscious rabbits in response to baroreceptor activation. Neurosci Lett. 1992; 144:70–74. [PubMed: 1359481]
22. Sved AF, Mancini DL, Graham JC, Schreihofer AM, Hoffman GE. PNMT-containing neurons of the C1 cell group express c-*fos* in response to changes in baroreceptor input. Am J Physiol Regul Integr Comp Physiol. 1994; 266:R361–R367.
23. Minson JB, Llewellyn-Smith I, Arnolda L, Pilowsky PM, Chalmers JP. *c-fos* expression in central neurons mediating the arterial baroreceptor reflex. Clin Exp Hypertens. 1997; 19(5–6):631–643. [PubMed: 9247744]
24. Li J, Potts JT, Mitchell JH. Effect of barodenervation on c-Fos expression in the medulla induced by static muscle contraction in cats. Am J Physiol. 1998; 274:H901–H908. (Heart Circ Physiol 3). [PubMed: 9530202]
25. Macefield VG, Henderson LA. Real-time imaging of the medullary circuitry involved in the generation of spontaneous muscle sympathetic nerve activity in awake subjects. Hum Brain Mapp. 2010; 31(4):539–549. [PubMed: 19777579]
26. Holt AG, Bissig D, Mirza N, Rajah G, Berkowitz B. Evidence of key tinnitus-related brain regions documented by a unique combination of manganese-enhanced MRI and acoustic startle reflex testing. PLoS One. 2010; 5(12):e14260. [PubMed: 21179508]
27. Bissig D, Berkowitz BA. Testing the calcium hypothesis of aging in the rat hippocampus in vivo using manganese-enhanced MRI. Neurobiol Aging. 2014; 35(6):1453–1458. [PubMed: 24439958]
28. Berkowitz BA, Roberts R, Bissig D. Light-dependant intraretinal ion regulation by melanopsin in young awake and free moving mice evaluated with manganese-enhanced MRI. Mol Vis. 2010; 16:1776–1780. [PubMed: 20808732]
29. Bissig D, Berkowitz BA. Manganese-enhanced MRI of layer-specific activity in the visual cortex from awake and free-moving rats. Neuroimage. 2009; 44(3):627–635. [PubMed: 19015035]
30. Mendonca-Dias MH, Gaggelli E, Lauterbur PC. Paramagnetic contrast agents in nuclear magnetic resonance medical imaging. Semin Nucl Med. 1983; 13(4):364–376. [PubMed: 6359418]
31. Yu X, Wadghiri YZ, Sanes DH, Turnbull DH. In vivo auditory brain mapping in mice with Mn-enhanced MRI. Nat Neurosci. 2005; 8(7):961–968. [PubMed: 15924136]
32. Inoue T, Majid T, Pautler RG. Manganese enhanced MRI (MEMRI): neurophysiological applications. Rev Neurosci. 2011; 22(6):675–694. [PubMed: 22098448]
33. Eschenko O, Canals S, Simanova I, Beyerlein M, Murayama Y, Logothetis NK. Mapping of functional brain activity in freely behaving rats during voluntary running using manganese-enhanced MRI: implication for longitudinal studies. Neuroimage. 2010; 49(3):2544–2555. [PubMed: 19896539]
34. Bade AN, Gendelman HE, Boska MD, Liu Y. MEMRI is a biomarker defining nicotine-specific neuronal responses in subregions of the rodent brain. Am J Transl Res. 2017; 9(2):601–610. [PubMed: 28337287]
35. Lu H, Yang S, Zuo Y, Demny S, Stein EA, Yang Y. Real-time animal functional magnetic resonance imaging and its application to neuropharmacological studies. Magn Reson Imaging. 2008; 26(9):1266–1272. [PubMed: 18448300]
36. de Sousa PL, de Souza SL, Silva AC, de Souza RE, de Castro RM. Manganese-enhanced magnetic resonance imaging (MEMRI) of rat brain after systemic administration of MnCl2: changes in T1 relaxation times during postnatal development. J Magn Reson Imaging. 2007; 25(1):32–38. [PubMed: 17173304]
37. Mueller PJ, Mischel NA. Selective enhancement of glutamate-mediated pressor responses after GABA(A) receptor blockade in the RVLM of sedentary versus spontaneous wheel running rats. Front Physiol. 2012; 3:447. [PubMed: 23189062]
38. Mueller PJ. Exercise training attenuates increases in lumbar sympathetic nerve activity produced by stimulation of the rostral ventrolateral medulla. J Appl Physiol. 2007; 102:803–813. [PubMed: 17053106]

39. Mischel NA, Llewellyn-Smith IJ, Mueller PJ. Physical (in)activity dependent structural plasticity in bulbospinal catecholaminergic neurons of rat rostral ventrolateral medulla. J Comp Neurol. 2014; 522(3):499–513. [PubMed: 24114875]
40. Subramanian M, Holt AG, Mueller PJ. Physical activity correlates with glutamate receptor gene expression in spinally-projecting RVLM neurons: A laser capture microdissection study. Brain Res. 2014; 1585:51–62. [PubMed: 25173073]
41. Llewellyn-Smith IJ, Mueller PJ. Immunoreactivity for the NMDA NR1 subunit in bulbospinal catecholamine and serotonin neurons of rat ventral medulla. Auton Neurosci. 2013
42. Eschenko O, Evrard HC, Neves RM, Beyerlein M, Murayama Y, Logothetis NK. Tracing of noradrenergic projections using manganese-enhanced MRI. Neuroimage. 2012; 59(4):3252–3265. [PubMed: 22119646]
43. Chuang KH, Koretsky AP. Accounting for nonspecific enhancement in neuronal tract tracing using manganese enhanced magnetic resonance imaging. Magn Reson Imaging. 2009; 27(5):594–600. [PubMed: 19144489]
44. Chuang KH, Koretsky A. Improved neuronal tract tracing using manganese enhanced magnetic resonance imaging with fast T(1) mapping. Magn Reson Med. 2006; 55(3):604–611. [PubMed: 16470592]
45. Allemang-Grand R, Scholz J, Ellegood J, Cahill LS, Laliberte C, Fraser PE, Josselyn SA, Sled JG, Lerch JP. Altered brain development in an early-onset murine model of Alzheimer's disease. Neurobiol Aging. 2015; 36(2):638–647. [PubMed: 25311279]
46. Silva AC, Lee JH, Aoki I, Koretsky AP. Manganese-enhanced magnetic resonance imaging (MEMRI): methodological and practical considerations. NMR Biomed. 2004; 17(8):532–543. [PubMed: 15617052]
47. Bissig D, Berkowitz BA. Same-session functional assessment of rat retina and brain with manganese-enhanced MRI. Neuroimage. 2011; 58(3):749–760. [PubMed: 21749922]
48. Van de Moortele PF, Auerbach EJ, Olman C, Yacoub E, Ugurbil K, Moeller S. T1 weighted brain images at 7 Tesla unbiased for Proton Density, T2* contrast and RF coil receive B1 sensitivity with simultaneous vessel visualization. Neuroimage. 2009; 46(2):432–446. [PubMed: 19233292]
49. Haase A. Snapshot FLASH MRI. Applications to T1, T2, and chemical-shift imaging. Magn Reson Med. 1990; 13(1):77–89. [PubMed: 2319937]
50. Berkowitz BA, Roberts R, Goebel DJ, Luan H. Noninvasive and simultaneous imaging of layer-specific retinal functional adaptation by manganese-enhanced MRI. Invest Ophthalmol Vis Sci. 2006; 47(6):2668–2674. [PubMed: 16723485]
51. Paxinos, G., Watson, C. The rat brain in stereotaxic coordinates. 6. Burlington, MA: Elsevier Inc; 2007.
52. Patel KP, Zhang K, Kenney MJ, Weiss M, Mayhan WG. Neuronal expression of Fos protein in the hypothalamus of rats with heart failure. Brain Res. 2000; 865:27–34. [PubMed: 10814730]
53. Zhang K, Zucker IH, Patel KP. Altered number of diaphorase (NOS) positive neurons in the hypothalamus of rats with heart failure. Brain Res. 1998; 786:219–225. [PubMed: 9555024]
54. Heesch CM, Zheng H, Foley CM, Mueller PJ, Hasser EM, Patel KP. Nitric oxide synthase activity and expression are decreased in the paraventricular nucleus of pregnant rats. Brain Res. 2009; 1251:140–150. [PubMed: 19041855]
55. Mueller PJ, Foley CM, Heesch CM, Cunningham JT, Zheng H, Patel KP, Hasser EM. Increased nitric oxide synthase activity and expression in the hypothalamus of hindlimb unloaded rats. Brain Res. 2006; 1115(1):65–74. [PubMed: 16938283]
56. Rorden C, Brett M. Stereotaxic display of brain lesions. Behav Neurol. 2000; 12(4):191–200. [PubMed: 11568431]
57. Berkowitz BA, Grady EM, Roberts R. Confirming a prediction of the calcium hypothesis of photoreceptor aging in mice. Neurobiol Aging. 2014; 35(8):1883–1891. [PubMed: 24680323]
58. Mueller PJ, Mischel NA. Selective enhancement of glutamate-mediated pressor responses after GABA(A) receptor blockade in the RVLM of sedentary versus spontaneous wheel running rats. Front Physiol. 2012; 3:447. [PubMed: 23189062]

59. Mueller PJ, Mischel NA, Scislo TJ. Differential activation of adrenal, renal, and lumbar sympathetic nerves following stimulation of the rostral ventrolateral medulla of the rat. Am J Physiol Regul Integr Comp Physiol. 2011; 300(5):R1230–R1240. [PubMed: 21346240]

60. Eschenko O, Evrard HC, Neves RM, Beyerlein M, Murayama Y, Logothetis NK. Tracing of noradrenergic projections using manganese-enhanced MRI. Neuroimage. 2012; 59(4):3252–3265. [PubMed: 22119646]

61. Aoki I, Naruse S, Tanaka C. Manganese-enhanced magnetic resonance imaging (MEMRI) of brain activity and applications to early detection of brain ischemia. NMR Biomed. 2004; 17(8):569–580. [PubMed: 15617055]

62. Chuang KH, Koretsky AP, Sotak CH. Temporal changes in the T1 and T2 relaxation rates (DeltaR1 and DeltaR2) in the rat brain are consistent with the tissue-clearance rates of elemental manganese. Magn Reson Med. 2009; 61(6):1528–1532. [PubMed: 19353652]

63. Grunecker B, Kaltwasser SF, Zappe AC, Bedenk BT, Bicker Y, Spoormaker VI, Wotjak CT, Czisch M. Regional specificity of manganese accumulation and clearance in the mouse brain: implications for manganese-enhanced MRI. NMR Biomed. 2013; 26(5):542–556. [PubMed: 23168745]

64. Itoh K, Sakata M, Watanabe M, Aikawa Y, Fujii H. The entry of manganese ions into the brain is accelerated by the activation of N-methyl-D-aspartate receptors. Neuroscience. 2008; 154(2):732–740. [PubMed: 18495352]

65. Klaassen CD. Biliary excretion of manganese in rats, rabbits, and dogs. Toxicol Appl Pharmacol. 1974; 29(3):458–468. [PubMed: 4283708]

66. Greenberg DM, Copp DH, Cuthbertson EM. Studies in Mineral Metabolism with the Aid of Artificial Radioactive Isotopes: VII. The distribution and excretion, particularly by way of the bile, of iron, cobalt, and manganese. J Biol Chem. 1943; 147:749–756.

67. Lee JH, Silva AC, Merkle H, Koretsky AP. Manganese-enhanced magnetic resonance imaging of mouse brain after systemic administration of MnCl2: dose-dependent and temporal evolution of T1 contrast. Magn Reson Med. 2005; 53(3):640–648. [PubMed: 15723400]

68. Bock NA, Paiva FF, Silva AC. Fractionated manganese-enhanced MRI. NMR Biomed. 2008; 21(5):473–478. [PubMed: 17944008]

69. Brozoski TJ, Ciobanu L, Bauer CA. Central neural activity in rats with tinnitus evaluated with manganese-enhanced magnetic resonance imaging (MEMRI). Hear Res. 2007; 228(1–2):168–179. [PubMed: 17382501]

70. Grassi G. Sympathetic neural activity in hypertension and related diseases. Am J Hypertens. 2010; 23(10):1052–1060. [PubMed: 20651696]

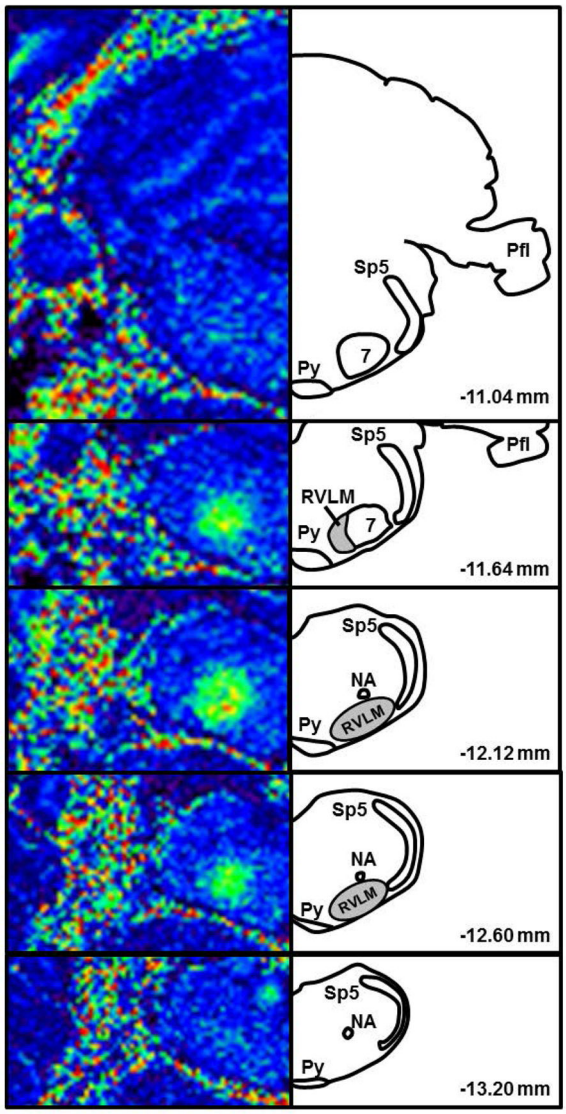

Figure 1. T_1-weighted images following proof-of-concept study utilizing microinjection of $MnCl_2$ into the pressor region of the RVLM

$MnCl_2$ (400 mM, 15 nl) was microinjected at the same coordinates used to functionally identify the RVLM by microinjection of glutamate (10 mM, 30 nl). MRI images (left) are matched rostrocaudally to diagrams drawn using a rat atlas for reference (right, Paxinos and Watson, 2007). In pseudocolored MR images, darker colors (blue) represent less Mn^{2+} enhancement and brighter colors (green, yellow, orange) represent greater Mn^{2+} enhancement. Shaded areas in diagrams represent the location of bulbospinal RVLM neurons (Schreihofer and Sved, 2011; Mueller and Llewellyn-Smith, 2013). Abbreviations: Sp5 = spinal trigeminal tract; 7 = facial nucleus; Py = pyramidal tract; NA = nucleus ambiguus; Pfl = paraflocculus; RVLM = rostral ventrolateral medulla.

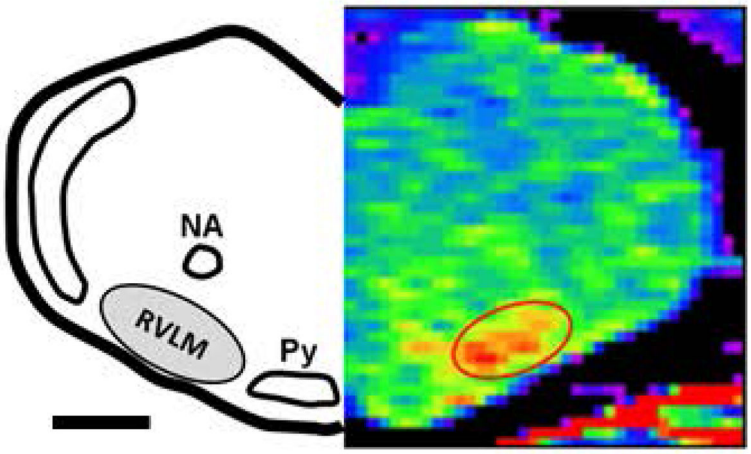

Figure 2. T_1-Map MEMRI image following proof-of-principle study utilizing microinjection of $MnCl_2$ (800 mM, 60nl) into the spinal cord at T9/T10

Animals were imaged 48 hours after spinal cord injection to allow for retrograde transport by bulbospinal RVLM neurons. MR image (right) is matched to a diagram drawn using a standard rat atlas for reference (left, Paxinos and Watson, 2007). Scale bar represents ≈ 1000 μm. Abbreviations and color scheme as described in Figure 1.

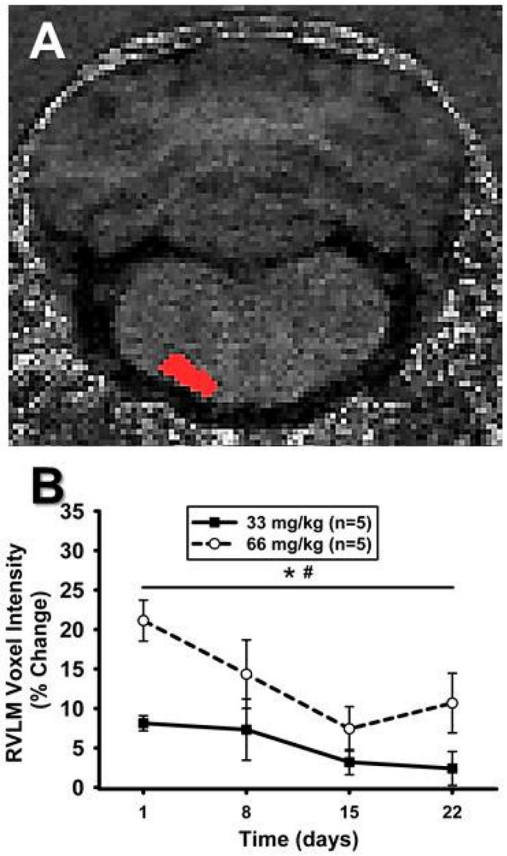

Figure 3. Mn^{2+} enhancement in the RVLM over time using T_1-weighted imaging

A) Unprocessed, non-colorized T_1-weighted MR image from one animal demonstrating detailed anatomy. ROI for the left RVLM is depicted in red and was used to determine voxel intensities in RVLM. **B)** Time course representing percent change in ROI mean voxel intensity in the RVLM following systemic injections of $MnCl_2$ at Day 0 (not shown) and calculated as a percent change from non-Mn^{2+}-injected baseline scans. ROI mean voxel intensity was highest at 24 hrs and significantly decreased over time in both groups (*, $p<0.05$ main effect of time). Voxel intensity was greater in animals injected with 66 mg/kg, compared to 33 mg/kg $MnCl_2$ (#, $p<0.05$ main effect of dose).

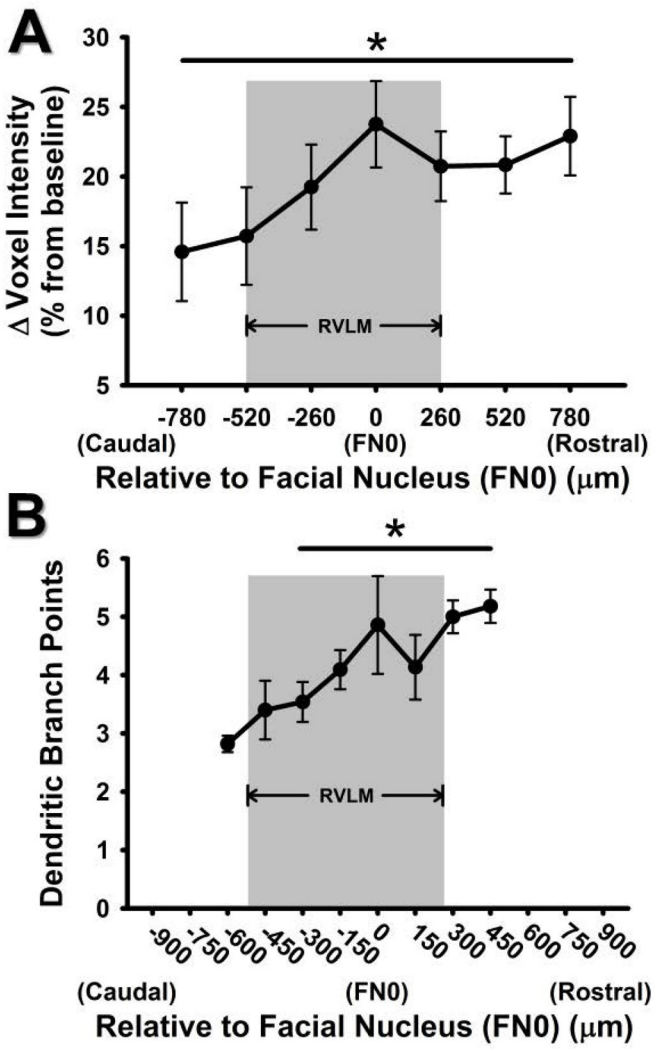

Figure 4. Comparison of caudal to rostral change in voxel intensity in the current study versus caudal to rostral change in dendritic branching from our previous study

A) Percent change in ROI mean voxel intensities of Mn^{2+} 24 hours after injection of 66 mg/kg $MnCl_2$, using T_1 weighted MRI scanning. The x-axis represents caudal to rostral axis of the ventrolateral medulla relative to the caudal pole of the facial nucleus (designated as FN0 and 0 μm). A pattern of increasing Mn^{2+} uptake was seen from the caudal to rostral levels of the RVLM (*, $p<0.05$, main effect). **B)** Pattern of increased dendritic branching from caudal to rostral areas of the ventrolateral medulla observed in bulbospinal catecholaminergic RVLM neurons from our previous study (*, $p<0.05$, compared to 600 μm; modified from Mischel *et al.,* 2014). Grey boxes represent the functionally and anatomically defined region of the RVLM.

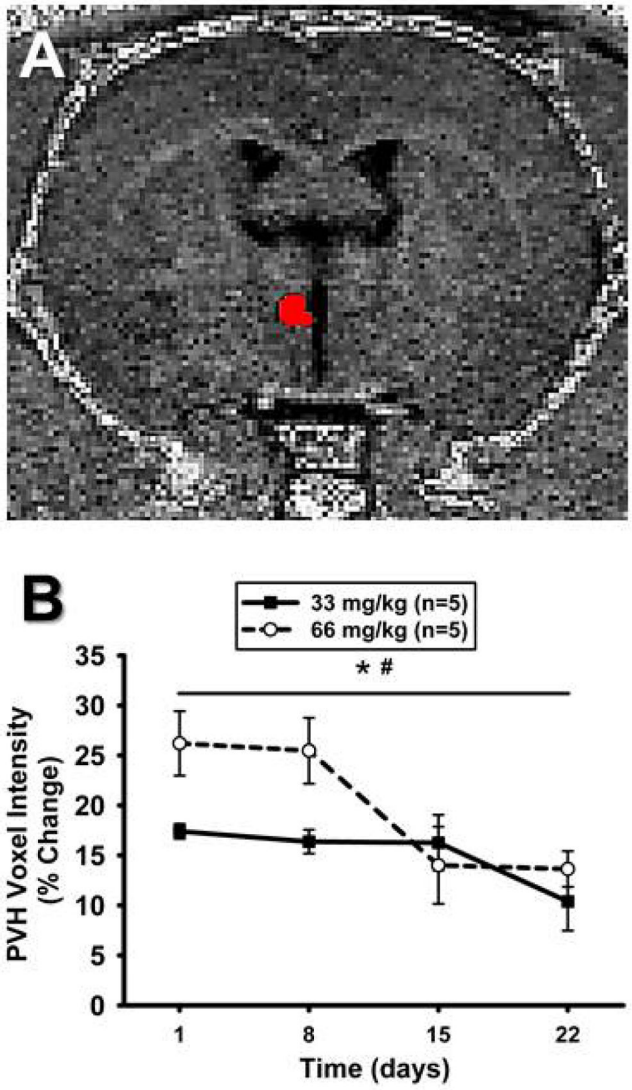

Figure 5. Mn^{2+} enhancement in the PVH over time using T_1-weighted imaging

A) Unprocessed, non-colorized T_1-weighted MR image from one animal demonstrating detailed anatomy. ROI depicted in red and was used to determine voxel intensities in the PVH. **B).** Time course representing percent change in ROI mean voxel intensity in the PVH following systemic injections of $MnCl_2$ at Day 0 (not shown) and calculated as a percent change from non-Mn^{2+}-injected baseline scans. ROI mean voxel intensity was highest at 24hrs and significantly decreased over time in both groups (*, $p<0.05$ main effect of time). ROI mean voxel intensity was greater in animals injected with 66 mg/kg, compared to 33 mg/kg $MnCl_2$ (#, $p<0.05$ main effect of dose).

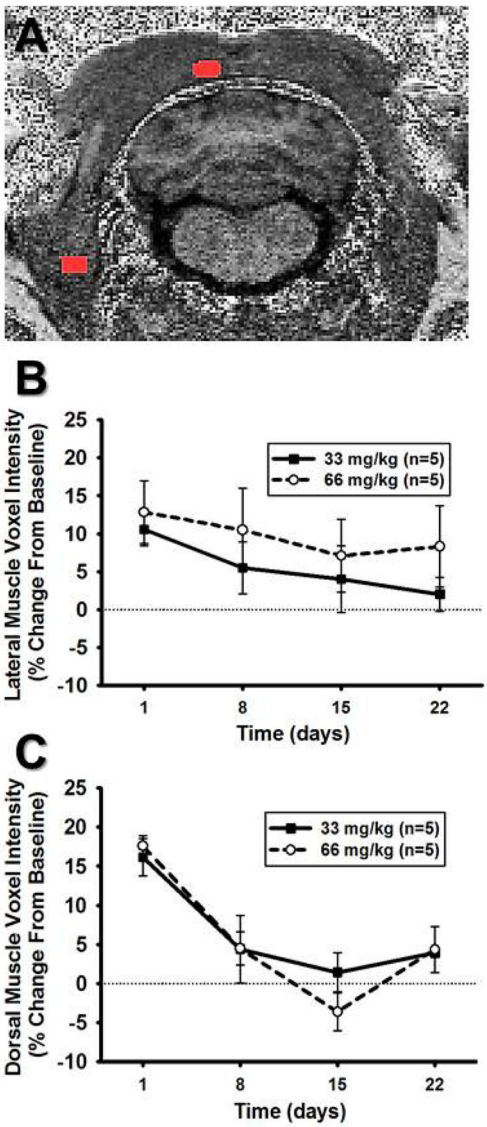

Figure 6. Mn^{2+} enhancement in muscle tissue surrounding the RVLM

A) Unprocessed, non-colorized T_1-weighted MR image from one animal demonstrating detailed anatomy. ROIs are depicted in red and were used to determine voxel intensities for the lateral muscle (splenius, lower lateral ROI) and dorsal muscle (cleidomastoid, upper midline ROI) regions. **B.)** ROI mean voxel intensity in the lateral muscle region expressed as percent change from baseline scans showed neither a significant main effect of dose nor time following injection of $MnCl_2$ ($p>0.05$, for both). **C)** ROI mean voxel intensity in the dorsal muscle region expressed as percent change from baseline scans following i.p. injection of $MnCl_2$ showed a significant effect of time (*, $p<0.05$, main effect of time) but showed no significant effect of dose ($p>0.05$, main effect of dose).

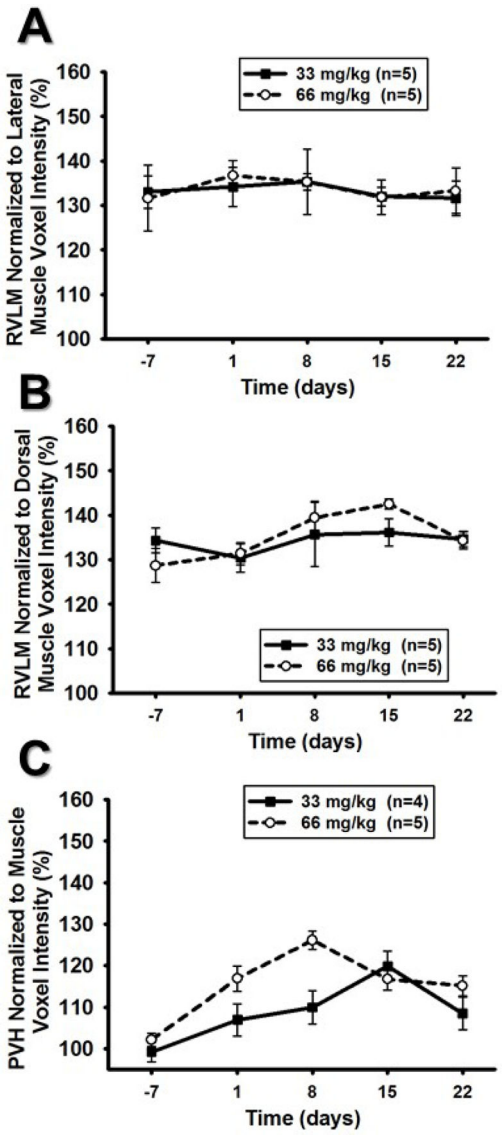

Figure 7. RVLM and PVH normalized to respective, adjacent muscle regions

A) RVLM ROI mean voxel intensity normalized to the lateral muscle tissue did not result in a significant dose or time effect ($p>0.05$ for both main effects). **B)** RVLM ROI mean voxel intensity normalized to the dorsal muscle tissue resulted in a small but significant time effect (*, $p<0.05$ main effect of time) but the patterns indicate an increase rather than a decrease in voxel intensity over time. RVLM ROI mean voxel intensity normalized to the dorsal muscle tissue did not result in an effect of dose ($p>0.05$ for main effect). **C.)** PVH ROI mean voxel intensity normalized to surrounding muscle tissue showed significant effect of dose (#, $p<0.05$) and time (*, $p<0.05$) however, the graph indicates an increase rather than decrease in voxel intensities over time.

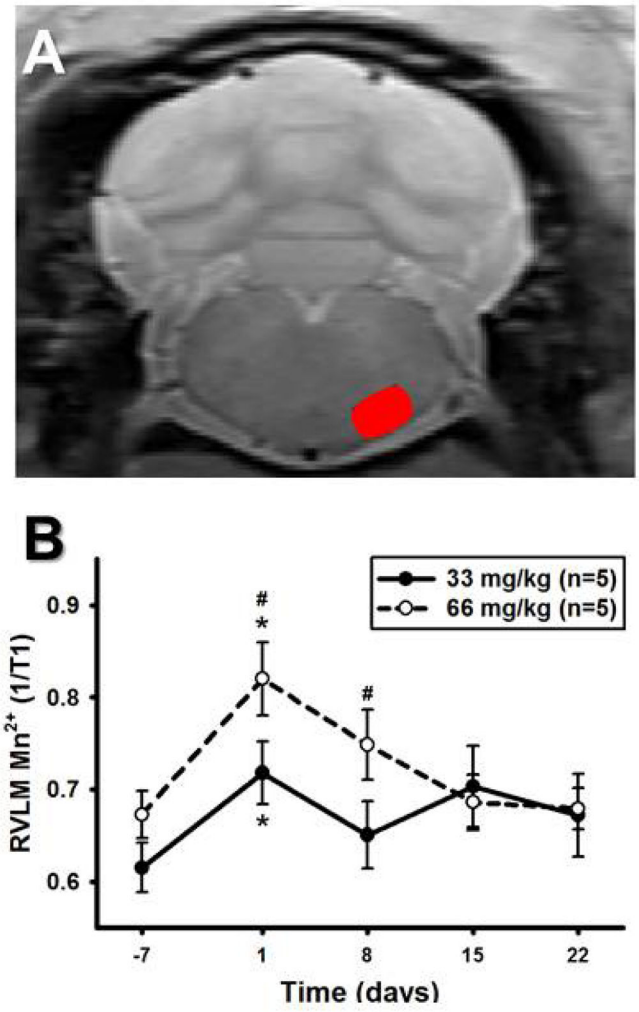

Figure 8. Mn^{2+} enhancement in the RVLM over time using T_1-mapping

A) Unprocessed, non-colorized T_1-mapping MR image from one animal demonstrating detailed anatomy. Red oval denotes outline of RVLM used for regions of interest (ROIs) calculations. **B)** RVLM $1/T_1$ values over time using T_1-mapping. After i.p. injections of 33 mg/kg or 66 mg/kg $MnCl_2$ (n=5 for both), there were significant main effects of time and dose for the RVLM $1/T_1$ ratio. A significant interaction between dose and time allowed post hoc testing to reveal significant increases in Mn^{2+} enhancement one day after $MnCl_2$ injection compared to the non-$MnCl_2$ injected baseline scan for both doses (*, $p<0.05$). Injections of 66 mg/kg resulted in greater Mn^{2+} enhancement compared to injections of 33 mg/kg $MnCl_2$ one and eight days after $MnCl_2$ injection (#, $p<0.05$).

Table 1

Time course of body weights of rats injected with 33 or 66 mg/kg $MnCl_2$

Time point	33 mg/kg $MnCl_2$ (n=5)	66 mg/kg $MnCl_2$ (n=5)
Prior to Baseline Scan (Day −7)	157 ± 11	155 ± 26
Prior to $MnCl_2$ injection (Day 0)	198 ± 11	185 ± 9
Prior to Day 1 scan	183 ± 8	177 ± 11
Prior to Day 8 scan	229 ± 6	215 ± 11
Prior to Day 15 scan	274 ± 6	260 ± 8
Prior to Day 22 scan	307 ± 4	291 ± 7

All weights are presented in grams as mean ± s.e.m.

Table 2

Time course of absolute voxel intensities in the pituitary of rats injected with 33 or 66 mg/kg $MnCl_2$.

	Absolute Voxel Intensity in the Pituitary Gland	
Time point	**33 mg/kg $MnCl_2$ (n=5)**	**66 mg/kg $MnCl_2$ (n=5)#**
Baseline Scan	1479 ± 29	1457 ± 34
1 day Scan	2689 ± 31 * (Δ 67±12%)	2758 ± 43 * (Δ 90±4%)
8 day Scan	2091 ± 109 * (Δ 33± 8%)	2279 ± 76 * (Δ 57±7%)
15 day Scan	1816 ± 39 * (Δ 20± 3%)	2008 ± 39 * (Δ 38±4%)
22 day Scan	1699 ± 26 * (Δ 13± 3%)	1823 ± 23 * (Δ 21±4%)

Absolute voxel intensities expressed in arbitrary units and percent change expressed relative to the Baseline Scan in each animals for each dose.

* $p<0.05$ main effect of time compared to baseline;

# $p<0.05$ main effect of dose.

Table 3

Time course of absolute voxel intensities obtained from T_1-weighted MRI scans of regions containing cerebrospinal fluid from rats injected with 66 mg/kg $MnCl_2$ (n=5).

Time point	Adjacent RVLM	Cerebral Aqueduct
Baseline Scan	566 ± 35	388 ± 31
1 day Scan	590 ± 11 (Δ 6 ± 5%)	401 ± 42 (Δ 5 ±10%)
8 day Scan	621 ± 19 (Δ11 ± 8%)	413 ± 27 (Δ 9 ± 9%)
15 day Scan	587 ± 31 (Δ 5 ± 6%)	410 ± 21 (Δ 7 ± 5%)
22 day Scan	614 ± 16 (Δ10 ± 7%)	413 ± 18 (Δ 9 ± 9%)